Received: 20 September 2017 | Revised: 01 February 2018 | Accepted: 05 March 2018 | Published on: 22 July 2018

DOI: 10.1002/qj.3284

RESEARCH ARTICLE

Quarterly Journal of the Royal Meteorological Society RMetS

The spatial distribution and temporal variability of föhn winds over the Larsen C ice shelf, Antarctica

Jenny V. Turton[1,2,3] | Amelie Kirchgaessner[1] | Andrew N. Ross[2] | John C. King[1]

[1]British Antarctic Survey, Cambridge, UK
[2]School of Earth and Environment, University of Leeds, Leeds, UK
[3]Insititut für Geographie, Friedrich-Alexander Universität, Erlangen-Nürnberg, Germany

Correspondence
Jenny V. Turton, Insititut für Geographie, Friedrich-Alexander Universität, Erlangen-Nürnberg, Germany.
Email: j.turton1990@hotmail.co.uk

The eastern side of the Antarctic Peninsula (AP) mountain range and the adjacent ice shelves are frequently affected by föhn winds originating from upwind of the mountains. Six automatic weather stations (AWSs) and archived model output from 5 km resolution Antarctic Mesoscale Prediction System (AMPS) forecasts have been combined to identify the occurrence of föhn conditions, and their spatial distribution over the Larsen C Ice Shelf (LCIS) from 2009 to 2012.

Algorithms for semi-automatic detection of föhn conditions have been developed for both AWS and AMPS data. The frequency of föhn varies by location, being most frequent at the foot of the AP and in the north of the ice shelf. They are most common in spring, when they can prevail for 50% of the time. The results of this study have important implications for further research, investigating the impact of föhn on surface melting, and the surface energy budget of the ice shelf. This is of particular interest due to the collapse of Larsen A and B ice shelves in 1995 and 2002 respectively, and the potential instability issues following a large calving event on Larsen C in 2017.

KEYWORDS

AMPS, Antarctic peninsula, boundary layer, foehn winds

1 | INTRODUCTION

The Antarctic Peninsula (AP) was the fastest warming region on Earth during the late 20th century, with air temperatures increasing at twice the global average (Vaughan *et al.*, 2003). Between 1995 and 2002, 3,200 km^2 of ice disintegrated from Larsen A and B ice shelves. Ice shelves are floating extensions of the land ice, and therefore their loss does not contribute to direct sea level rise. However, indirect sea level rise is a concern due to the acceleration of the glaciers feeding into the embayments (Scambos, 2004).

The proximal cause of this destabilization is the deepening of crevasses by the intrusion of melt water, often referred to as the "hydrofracture mechanism" (Scambos *et al.*, 2000). The outward pressure from the water-filled crevasse can overcome the inward pressure to close it. The "föhn hypothesis" proposes that the loss of Larsen A and B ice shelves was associated with an increased frequency of föhn winds driven by a positive trend of westerly winds, which led to a increase in surface melt (Marshall *et al.*, 2006).

Föhn winds are warm, dry, downslope winds in the lee of steep obstacles, such as the AP, where prevailing air flow is roughly perpendicular to the mountain range. The onset of föhn is often associated with a decrease in relative humidity and/or a simultaneous increase in temperature. Once the föhn has developed, the dry, warm conditions can persist for a number of hours or even days. In a number of cases, especially during the extended summer months (October to April), föhn winds can raise the surface temperature of the Larsen C Ice Shelf (LCIS) sufficiently to initiate surface melt.

There are two dominant mechanisms responsible for the development of föhn winds. The first, the "thermodynamic theory" of Hann (1866), describes the adiabatic heating and drying of air parcels, when air impinges on a barrier. Air parcels from lower altitudes rise up the windward side of a mountain, and cool at the saturated adiabatic lapse rate. This leads to condensation and precipitation on the windward side. Once the barrier is overcome, the now drier air parcel descends on the leeside of the obstacle, and warms at the higher dry adiabatic lapse rate, leading to warmer and drier conditions in the lee.

The second mechanism is isentropic drawdown. In this case, low-level blocking on the windward side leads to high-altitude air interacting with the mountain. Advection of potentially warmer and drier air from aloft towards the surface generates the föhn conditions (Elvidge and Renfrew, 2016). Turbulent sensible heating, mechanical mixing of air on the lee slope, and increased incoming solar radiation from cloud-clearing can also enhance föhn warming (Miltenberger *et al.*, 2016). In this study, two methods of detection have been used to identify föhn conditions from observations and from the Antarctic Mesoscale Prediction System (AMPS). Due to the method used with the AMPS data, the föhn conditions reported here primarily originate from the isentropic drawdown mechanism. However, föhn winds generated by both isentropic drawdown and thermodynamic processes will be characterized by cross-barrier warming (King *et al.*, 2017).

A number of studies have recently focused on investigating the impact of föhn conditions and katabatic winds on ice shelves around Antarctica. In-depth case-study analyses have highlighted the impact that föhn winds have on the near-surface conditions and surface energy balance of the LCIS through observations and modelling (Elvidge *et al.*, 2015; King *et al.*, 2015; 2017; Elvidge and Renfrew, 2016; Turton *et al.*, 2017). Furthermore, Lenaerts *et al.* (2017) and Grazioli *et al.* (2017) have analysed the contribution of katabatic winds to the mass balance and melt production on ice shelves using both observations and models. Similarly, Luckman *et al.* (2014) and Hubbard *et al.* (2016) identified the link between surface and internal ice-shelf processes (melt ponds, densification, loss of firn air) and wind-driven processes such as föhn and katabatic winds.

Whilst the understanding of the interaction between föhn winds and the ice-shelf surface is becoming deeper, there still remain gaps in the knowledge of the occurrence and frequency of föhn winds over the LCIS. Cape *et al.* (2015) presented a climatology of föhn frequency and conditions over the northern AP, but, up to now, our knowledge of the temporal and spatial distribution of föhn conditions over the LCIS was restricted to case-studies. The present study combines observations from five sites on the LCIS and one on the remnants of Larsen B, with modelling output at 5 km horizontal resolution to provide a detailed analysis of the frequency of föhn conditions, and of the spatial distribution of föhn winds over four years. Without understanding the frequency and temporal distribution of föhn conditions, analyses of their climatological contribution to surface melt remain uncertain.

2 | DATA DESCRIPTION

2.1 | Study area

The LCIS is part of the larger Larsen ice shelf group, comprised of Larsen A, B, C and D (north to south), on the eastern side of the AP (Figure 1). The LCIS is characterized by a flat, shallow sloping surface, with deep crevasses and persistent summer melt ponds to the northwest (Luckman *et al.*, 2014). To the west of the ice shelf, the steep, narrow mountain range of the AP acts as a barrier to warm, moist airflow from the west. Consequently, air temperatures over LCIS are up to 10°C cooler than at the same latitude on the west (Morris and Vaughan, 2003). The AP mountains also act to initiate the development of föhn winds.

In July 2017, roughly 10% of the ice area calved from LCIS, after rapid propagation of a rift since 2013 (Hogg and Gudmundsson, 2017). LCIS is now at its areal minimum since at least the beginning of observations, but possibly since the beginning of the holocene (Jansen *et al.*, 2015). Although calving events are natural processes, LCIS is being closely monitored for signs of destabilization similar to Larsen B (Cook and Vaughan, 2010).

2.2 | Near-surface data

Near-surface meteorological data were obtained from six Automatic Weather Stations (AWSs) located on the LCIS and adjacent AP (Figure 1). AWS1, 2 and 3 are operated by the Institute for Marine and Atmospheric Research Utrecht (IMAU). AWS5 and 6 were operated by the Cooperative Institute for Research in Environmental Science (CIRES) at the University of Colorado. The final AWS, referred to as "Cole Peninsula" or "CP" was deployed as part of the Orographic Flow and the Climate of the Antarctic Peninsula (OFCAP) field campaign in January 2011 by the British Antarctic Survey (BAS). Table 1 describes the location, elevation and observed variables for each AWS used by this study.

The AWS observations have been centre-averaged into six-hourly data points, centred on 0000, 0600, 1200, 1800 UTC from January 1, 2009 to December 31, 2012 for comparison with model output. The use of six-hour averaged data is not thought to influence the results, as other föhn studies in this region regularly identified föhn events of over 24 hr in duration (Cape *et al.*, 2015; Elvidge *et al.*, 2016).

2.3 | AMPS

Model output used in this project was obtained from the Antarctic Mesoscale Prediction System (AMPS). This is a numerical weather prediction (NWP) tool for the Antarctic that is based on the Weather Research and Forecasting (WRF)

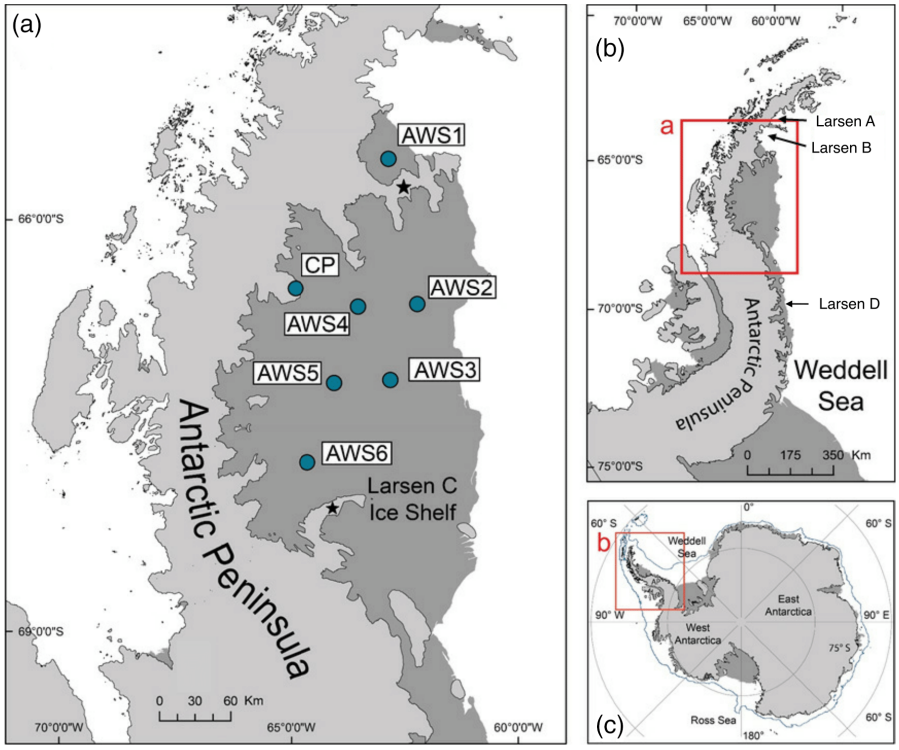

FIGURE 1 (a) Map of the Larsen C ice shelf with AWS locations and names. CP is the the Cole Peninsula AWS. The two black stars refer to Jason Peninsula (top) and Kenyon Peninsula (bottom) which can cause localized föhn features. (b) Map of the Antarctic Peninsula with the Larsen Ice Shelf highlighted by the red box a. Larsen A and B embayments are labelled with arrows. (c) Map of the Antarctic continent with the Antarctic Peninsula highlighted by the red box b. Coastlines imported from the Antarctic Digital Database [Colour figure can be viewed at wileyonlinelibrary.com]

mesoscale model, and is operationally run by the National Center for Atmospheric Research (NCAR), USA. Complementing observational data with model output is particularly useful over the Antarctic continent due to sparse observation networks. However the sparse observation network can mean that forecast models are not well contained or verified in this region, which can be a challenge (Bromwich *et al.*, 2009). The observational data used in this project were not assimilated by AMPS, and therefore the AMPS model output is independent of the observations.

From 2006 until 2011, AMPS was implemented using the standard versions of the WRF model. Since January 2011 "Polar WRF" version 3.0.1 was used within AMPS. Global Forecast System (GFS) data were used to force the lateral boundaries, and the model was initialized twice daily at 0000 and 1200 UTC (Hines and Bromwich, 2008). Polar WRF is a modified version of WRF to better represent both the polar regions (Wilson *et al.*, 2012). Output from AMPS domain 6, run and archived by National Center for Atmospheric Research (NCAR), was used within this project as it is centred on the AP. This domain has a 5 km horizontal resolution (346 × 301 points), 44 vertical terrain-following levels and is nested within a larger domain covering the Antarctic continent. King *et al.* (2015) give more information. AMPS has previously been used for Antarctic föhn studies by Steinhoff *et al.* (2014) and Cape *et al.* (2015). The AMPS model performs relatively well at representing the near-surface conditions over the Larsen C. In the King *et al.* (2015) study, mean biases

TABLE 1 AWS metadata for the six available stations

AWS no. (ownership)	Location	Height amsl (m)	Parameters observed	Dates available
Cole Peninsula (BAS)	66.85°S, 63.80°W	420	T, RH, FF, DD, P	21/01/2011–08/01/2012
AWS1 (IMAU)	65.93°S, 61.85°W	50	T, RH, FF, DD, P, SW↓, SW↑, LW↓, LW↑	19/02/2011–11/03/2014
AWS2 (IMAU)	67.02°S, 61.50°W	50	T, RH, FF, DD, P, SW↓, SW↑, LW↓, LW↑	22/01/2009–11/03/2014
AWS3 (IMAU)	67.57°S, 62.15°W	50	T, RH, FF, DD, P, SW↓, SW↑, LW↓, LW↑	21/01/2009–11/03/2014
AWS5 (CIRES)	67.57°S, 63.26°W	42	T, RH, FF, DD, P, SW↓, SW↑, NetRad	22/12/2008–15/11/2011
AWS6 (CIRES)	68.14°S, 63.95°W	53	T, RH, FF, DD, P	24/12/2008–26/12/2012

BAS is the British Antarctic Survey, IMAU is the Institute of Marine and Atmospheric Research, University of Utrecht and CIRES is the Cooperative Institute for Research in Environmental Sciences, University of Colorado. T=air temperature, RH=relative humidity, FF=wind speed, DD=wind direction, P=pressure, SW↑=outgoing short-wave radiation, SW↓=incoming short-wave radiation, LW↑=outgoing long-wave radiation, LW↓=incoming long-wave radiation, NetRad=net radiation.

of ~ -1 K for air and surface temperature were identified in AMPS, however the model was found to overpredict melt episodes due to a positive bias in incoming short-wave radiation and a low albedo value. Supplementary Tables S1 and S2 give details of how AMPS performs for the locations and period in this article. Archived AMPS output for domain 6 from January 1, 2009 to December 31, 2012 has been used in the current study.

Model data have been extracted for all AWS locations, using the coordinates of the AWS, with the exception of Cole Peninsula (67.0°S, 64.2°W). An approximate location was used for Cole Peninusla as the exact geographical co-ordinates within the AMPS domain did not correspond to a similar altitude. The 'pseudo-location' chosen was 66.8°S, 64.1°W, as this location in the model was at a more representative altitude (Supplement Table S3 gives more information).

2.4 | AWS föhn identification algorithm

Selecting thresholds to identify föhn within the lee remains a common method when a mountain-top AWS is not available. A mountain-top AWS would allow the potential temperature to be observed and compared with a valley-bottom AWS, as used in numerous Alpine valleys (Dürr, 2003; Vergeiner, 2004), although this method still incorporates thresholds. The AWS algorithm presented here was used and tested in a case-study analysis of föhn winds at two locations (Cole Peninsula and AWS2) over the LCIS by Turton *et al.* (2017). In this article, the algorithm has been further developed and adapted for use at the other AWS locations. The method is similar to others used in the Alps (Richner *et al.*, 2005; Gaffin, 2007) and over the Antarctic (Speirs *et al.*, 2013). The chosen thresholds reflect the characteristics of the föhn conditions over the LCIS, and are therefore specific for this region.

A number of known, and extensively analysed, föhn events from Elvidge *et al.* (2015; 2016) and King *et al.* (2017) were assessed, and the average relative humidity during these events was used as a basis for the thresholds used below. A time point was flagged as "föhn" if at least one of the thresholds was met:

1. A decrease of X% relative humidity over 12 hr (RH12h). X varied depending on the location of the AWS (Table 2). This threshold is based on those used in Cape *et al.* (2015) over the northern AP. The use of the 12 hr time frame removed the possibility of incorporating slower, synoptic changes into the algorithm.
2. Relative humidity below the 10th percentile value (RH10P). Using percentiles rather than absolute values allows this algorithm to be applicable for the whole LCIS. For example, the 10th percentile at Cole Peninsula was much lower than other locations as the average conditions were drier. The thresholds are based on analysis of previously published föhn events over the LCIS.
3. Relative humidity below the 15th percentile value combined with a temperature increase of $\geq$3.0 K over 12 hr (RH15P). An increase in temperature often accompanies föhn onset, however this signal can be masked. During summer, the increased incoming solar radiation weakens the temperature response to föhn onset (Cape *et al.*, 2015). This threshold removes any bias caused by seasonal temperature fluctuations, and incorporates a higher relative humidity percentile to identify föhn conditions with slightly weaker characteristics.

Föhn conditions close to the AP (at Cole Peninsula and AWS1 for example) can be considered binary. The low relative humidity observed throughout föhn events cannot be reproduced by other conditions (such as dry continental air). In sensitivity studies, when the relative humidity thresholds were increased to the 20th percentile of relative humidity values, the number of föhn conditions increased by only 4%. Further east, the situation was similar. Varying the relative humidity threshold to between 60 and 80% altered the number of föhn conditions by a maximum of 13%. Thus, varying the thresholds used for this method has a limited impact on the number of föhn conditions identified.

Closer to the AP, the föhn conditions were stronger, and their onset was marked by a greater change in relative humidity. For example a föhn event which was observed at both Cole Peninsula (foot of the mountains) and AWS2 ($\sim$100 km further east) is displayed in Figure 2. The thresholds reflect the varying föhn signal and are therefore specific to each location (Table 2).

The temperature change associated with föhn onset at each AWS location was more spatially homogeneous than the relative humidity change, and therefore the temperature change threshold was the same for all locations. A change in temperature must have been identified in conjunction with a relative humidity decrease, as the temperature change was not, on its own, an indicator of föhn air. The relative humidity thresholds had a greater precedence than the temperature signal in this method, to remove any seasonal bias.

2.5 | AMPS föhn identification algorithm

The AMPS algorithm was not analogous to the AWS one, as the near-surface conditions were not used for föhn identification. Instead, the method used here, developed by Bannister (2015) for over South Georgia and used previously by Turton *et al.* (2017), and King *et al.* (2017) is based on the disturbance to the potential temperature field from the interaction of the air flow and the AP. This method isolates the isentropic drawdown (Figure 3), which is one of the dominant mechanisms for AP föhn events (Elvidge and Renfrew, 2016). The AMPS föhn identification algorithm is summarized below and in Figure 3. King *et al.* (2017) gives a more detailed description.

- Take west to east cross-sections through the AP, at latitudes corresponding to the AWS locations (Table 3),

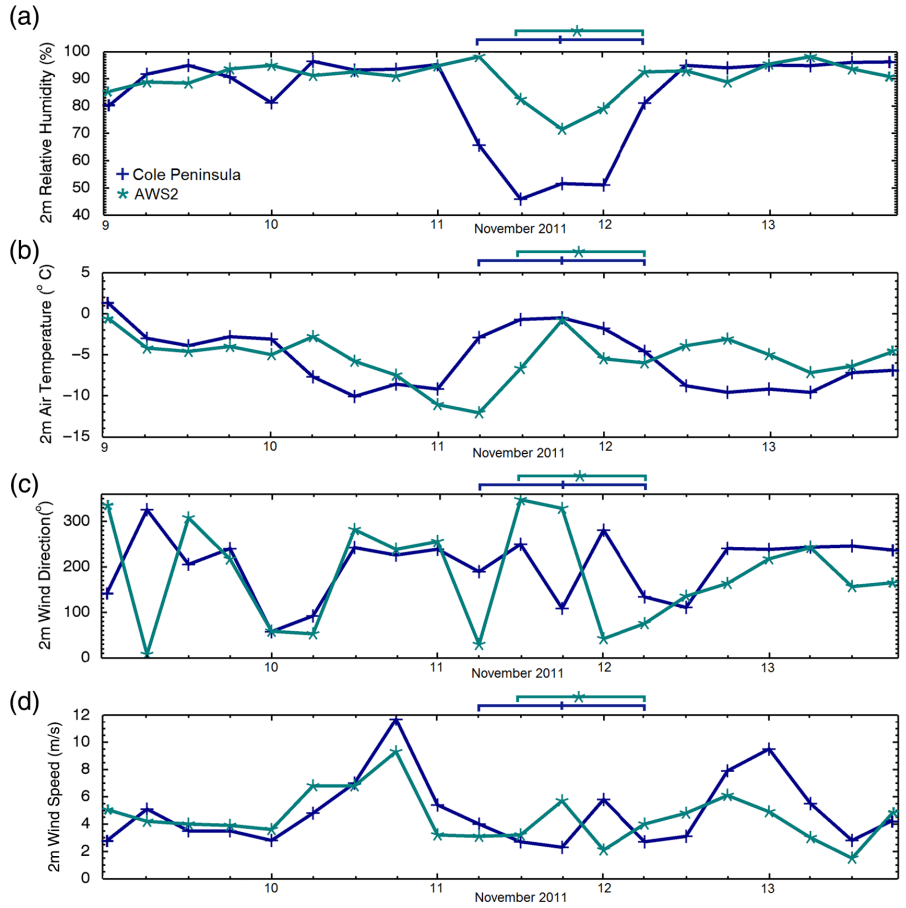

FIGURE 2 The near-surface meteorological response to föhn conditions from November 9 to 13, 2011: (a) 2 m relative humidity, (b) air temperature, (c) wind direction and (d) wind speed. Cole Peninsula observations are dark blue (+), and AWS2 observations are teal (*). The dark blue (Cole Peninsula) and teal (AWS2) lines above each panel indicate the identification of a föhn event from the AWS identification algorithm [Colour figure can be viewed at wileyonlinelibrary.com]

TABLE 2 Humidity thresholds that must be met for föhn conditions to be identified at any time point using the AWS algorithm

AWS	RH10P	RH15P	RH12h
Cole Peninsula	51.8%	58.5%	>17.5%
AWS1	67.3%	74.1%	>15%
AWS2	72.6%	78.7%	>15%
AWS3	76.9%	81.3%	>15%
AWS5	75.2%	80.1%	>15%
AWS6	77.4%	82.4%	>10%

TABLE 3 The location-specific thresholds used in the AMPS algorithm to identify föhn conditions at each location within the model output

AWS	θ_{up} longitude	θ_{up} latitude	$h1$ (m)	x
Cole Peninsula	70°W	66.8°S	2,000	65–63°W
AWS1	68°W	65.9°S	1,700	63–61°W
AWS2	70°W	67.0°S	2,000	65–63°W
AWS3	70°W	67.6°S	1,500	66–64°W
AWS5	70°W	67.6°S	1,500	66–64°W
AWS6	69°W	68.1°S	1,500	66–64°W

θ_{up}, $h1$ and x are explained in the text.

- for each model time and each cross-section, isolate the potential temperature (θ_{up}) at an elevation just above the height of the AP ($h1$), in undisturbed, upwind flow (~70°W).
- isolate θ_{up} again, due east of the up-barrier location, in the lee, within 2° longitude of the AP (x).
- determine the minimum elevation of θ_{up} within this longitude range.

Conditions were flagged as "föhn" when the following was satisfied:
the altitude of the isentrope θ_{up}, from up-barrier (undisturbed) to leeside, descended by 500 m or more ($h2$).

The value of θ_{up} was selected at approximately AP height, which varied from 2,000 to 1,500 m in this region. The decrease in altitude of the isentrope in the lee must have been significant to provide the warming and drying towards the surface of the LCIS, therefore 500 m below the AP height was used. In a sensitivity test (not shown), the 1,000 m descent used by Bannister (2015) was applied. However, this identified very few föhn conditions. This method was also applied in King *et al.* (2017), where the choice of thresholds is discussed. The location-specific thresholds are displayed in Table 3.

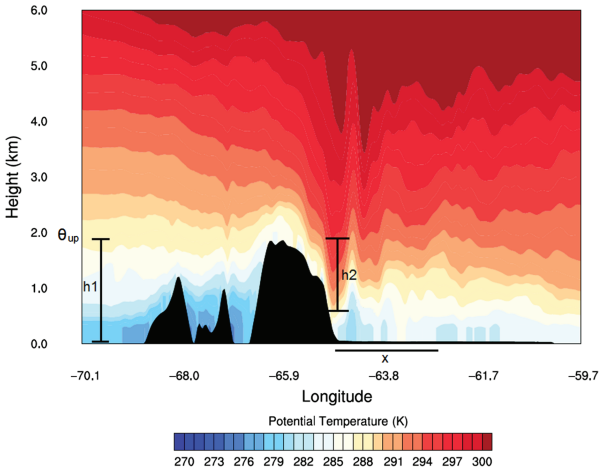

FIGURE 3 Cross-section of the modelled potential temperature at 67°S during a typical föhn, with annotations to describe the AMPS algorithm method.(θ_{up}) is the upwind potential temperature at the height ($h1$) of the AP, in undisturbed flow. $h2$ is the descent of θ_{up} in the lee of the AP. The location of interest is x

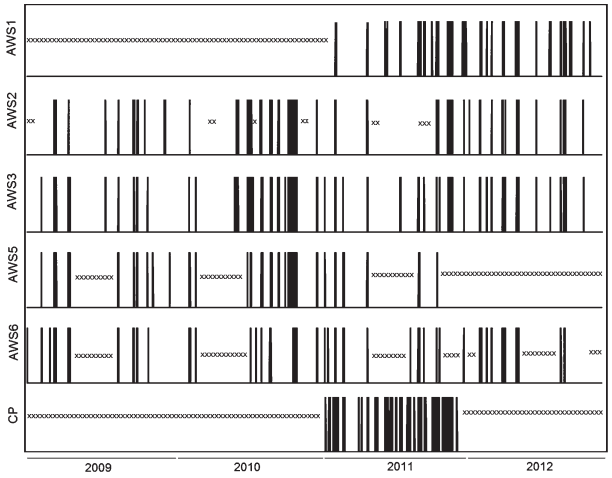

FIGURE 4 The föhn frequency barcode. The frequency of föhn conditions at each location, as identified by the AWS and AMPS algorithms, from 2009 to 2012. The black bars are the 6 hr föhn conditions. 'x' indicates periods where at least 72 consecutive hours of data are missing

2.6 | Algorithm combination

From both the AWS and AMPS algorithms, a number of time points were flagged as fulfilling the required criteria, and therefore possessing a föhn signature. Primarily, föhn conditions have been identified from near-surface characteristics observed by the AWSs. The AMPS algorithm has then been used to confirm that flow during these periods was cross-barrier, with significant isentropic drawdown and therefore of föhn origin. The two algorithms have been combined to ensure that föhn characteristics were present in both the near-surface and the upper-air data.

To combine the two algorithm results, a "hit" test was performed. A "hit" was a föhn that was identified by both the AWS and AMPS algorithm. From 2009 to 2012, there were 878 hits identified from all locations. Föhn conditions that were identified by only one algorithm were not classed as hits.

At all locations over four years, the AMPS algorithm detected 2,300 more föhn conditions than were identified at the surface by the AWS algorithm, highlighting the potential dominance of the isentropic drawdown mechanism in this region. For 12% of these "AMPS only" cases, the AWS algorithm identified the same föhn conditions as the AMPS algorithm, but there was up to a 12 hr lag between the algorithms. These cases were not taking into account within the results, or analysed further, since to include a time-lag between the algorithms could increase the subjectivity of the methods. For 11% of the time period analysed, the AWS algorithm detected föhn conditions near the surface and the isentropic drawdown signature was present, but was not close enough to the surface to reach the AMPS algorithm threshold. Therefore, more föhn conditions may have been present on the ice shelf, but were not included in the analysis as they did not meet the criteria. As the two algorithms identified different processes, a high hit number was not a measure of the two algorithms' success. It was instead used as a way of ensuring that those föhn conditions used for further analysis possessed both surface and upper-air signatures that are characteristic of föhn winds. In total, the algorithms agreed on either föhn (hit) or non-föhn conditions 80% of the time. For the remainder of this article, only föhn conditions identified by both algorithms were included in further analysis. We define "föhn conditions" as the individual times identified as föhn, and "föhn events" as periods of continuous föhn conditions.

3 | RESULTS

3.1 | Temporal variability

As a total of all locations, from 2009 to 2012, 878 föhn conditions were identified, accounting for approximately 15% of the time (Figure 4). The number of föhn identified within each year varied. The least number of föhn were identified in 2009 (134 föhn conditions) (Table 4). The highest number of identified föhn conditions occurred in 2011 (356 föhn conditions). However, there were six operational AWSs during this year, including Cole Peninsula, which had more föhn conditions identified than elsewhere. When excluding the Cole Peninsula results, a total of 165 föhn conditions were identified in 2011, which was comparable with the other years.

There was a clear seasonal peak in the number of föhn identified. Considerably more föhn conditions were identified during spring (September, October, November) than autumn and summer. In 2010, over 65% of identified föhn conditions occurred during spring. On average, 54% of spring days experienced at least one föhn condition.

The duration of föhn events ranged from 6 to 72 hr, with a median duration of 12 hr. Based on our data, föhn events could not be shorter than 6 hr due to the averaging used. Six-hour events were the most frequent, accounting for 48% of the 428 total föhn events. The longest event (72 hr) was identified at Cole Peninsula. The longest period with temperatures above

TABLE 4 The number of föhn conditions identified at each AWS for each year of available data

Location	2009	2010	2011	2012	AWS average
CP	ND	ND	191	ND	191
AWS1	ND	ND	58	65	62
AWS2	22	51	21	30	31
AWS3	32	69	32	37	43
AWS5	38	45	20	ND	34
AWS6	42	29	34	62	42
Annual average	34	49	59	49	—

ND indicates no data for an entire year.

freezing was during a 66 hr föhn event (February 23–25, 2011). Föhn events in winter (13.0 hr) were longer than in other seasons (12.1 hr), although the difference is not statistically significant. Winter also experienced the highest number of föhn events lasting for more than 24 hr.

Figure 4 displays the föhn conditions identified at each location throughout the study period. The intermittent nature of the föhn conditions is clear, creating a "barcode" style pattern, with a congregation of föhn conditions over a few weeks or months. The impact of individual föhn conditions was often short-lived and localized. However periods of consecutive, or multiple föhn events cause an aggregation of the warming which may create a longer-lasting impact.

3.2 | Spatial distribution

Föhn conditions were identified at all six locations across the LCIS. The specific frequency, strength and near-surface characteristics of the föhn conditions varied by location. As Cole Peninsula was at the foot of the AP, even weak föhn conditions could be observed here, which subsequently lead to a higher frequency of föhn conditions. AWS1 identified the second highest number of föhn conditions, 62 per year on average. This location is furthest north, on the remnants of Larsen B ice shelf, and was the closest to the AP after Cole Peninsula.

Föhn conditions were identified as far south as AWS6 (68.14°S, 63.95°W). This is the furthest south that föhn conditions have been observed over the LCIS. This displays the potential for föhn-induced melt closer to the Antarctic continent, and further south than previously expected from analysis of föhn-related melt ponds from satellite data (Luckman *et al.*, 2014). Over 24% of all föhn conditions were identified at more than one location (multi-location föhn conditions), and 37 föhn conditions were identified by all active stations at the same time (four or more locations). This was not unexpected as the föhn air propagates across the LCIS, from close to the AP, eastwards where it mixes with cooler and moister air. Föhn conditions were still frequently identified at AWS2 and 3 despite their distance from the AP.

3.3 | Near-surface characteristics

Of the 191 föhn conditions identified at Cole Peninsula, only 37% were simultaneously identified elsewhere. Due to its close proximity to the AP, even weak föhn winds were identified at this location. Despite the relatively localized distribution of the föhn conditions identified at Cole Peninsula, they have a wider-reaching impact on the ice shelf.

The average near-surface conditions at all locations during Cole Peninsula's föhn events were RH= 48% and T = −13.0 °C. Conversely, during non-föhn periods at Cole Peninsula, the shelf-wide mean T was −3.5 K lower and RH was 94.5%. The largest average change in air temperature was +4.2 °C at AWS3, which was located over 100 km from Cole Peninsula. Therefore, even when föhn conditions were only identified at the foot of the mountains, they affected the whole ice shelf.

Incorporating all föhn conditions from 2009 to 2012 leads to a larger change in conditions. All locations observed a mean decrease in RH of at least 19% and a mean T increase of at least 11 K when comparing composites of non-föhn with föhn conditions. The clear shifts from moist, cold non-föhn conditions, to significantly drier and warmer föhn conditions are presented in Figure 5.

The magnitude of the RH and T change at a location was related to the distance from the AP and latitude. As air propagated southeastward from the AP, the föhn signal weakened due to the mixing with moister ambient air. An approximate west–east gradient in decreasing föhn signal was identified during multi-location föhn conditions, and to some extent during a composite of all föhn conditions (Figure 6). An approximate north–south gradient in decreasing strength was also identified in observations of both RH and T, however AWS6 had a lower RH than further north at AWS5 and AWS3.

Although AMPS does not always represent the near-surface conditions accurately over the ice (King *et al.*, 2015), it does provide some measure of the spatial extent and variability in föhn conditions which is hard to obtain with the limited number of AWS observations. As evident in Figure 7, a composite of all föhn conditions from 2009–2012, there was a northwest to southeast gradient in decreasing föhn strength (increasing RH and decreasing T) over the LCIS.

4 | DISCUSSION

Dry, warm, föhn conditions have been observed over the whole of LCIS, stretching 260 km in a north–south direction and up to 130 km east of the AP. The föhn winds were identified in near-surface AWS observations and in archived 5 km resolution model output. This is the first study to investigate the spatial distribution and temporal features of föhn over the whole LCIS. This study has implemented and expanded on a relatively new method for identifying föhn from AWS and AMPS data.

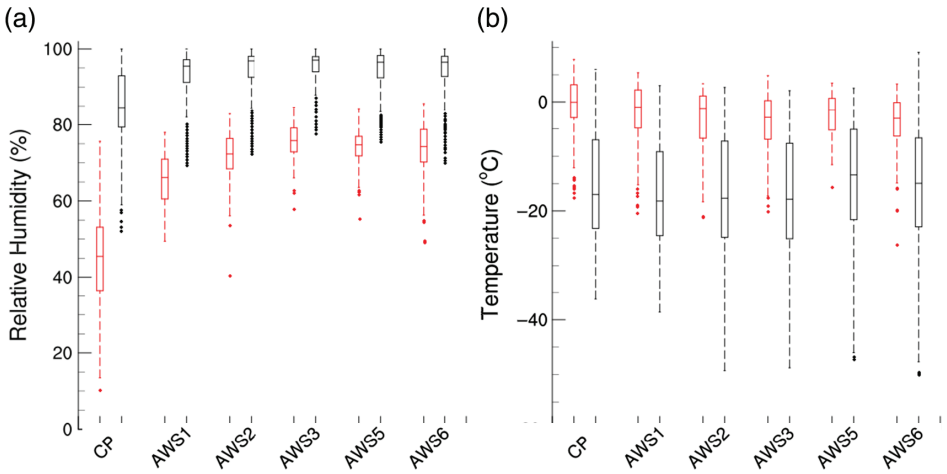

FIGURE 5 Average föhn (red) and non-föhn (black) (a) relative humidity and (b) air temperature conditions observed at each location. The box represents the 25th, 50th and 75th quartile values. The whiskers extend to the minimum and maximum values (dashed lines). Outliers are dots

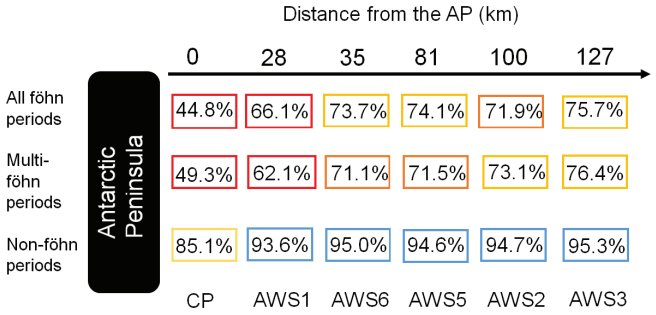

FIGURE 6 The average relative humidity observed at each location during föhn conditions (top), multi-location föhn conditions (middle) and non-föhn periods (bottom) The colours aid with displaying the decreasing föhn signal

The results of this study rely, in part, on the accurate representation of upper-air flow in AMPS. As AMPS has previously been found to represent near-surface conditions relatively well (e.g. King *et al.*, 2015), and has been used in previous föhn wind studies (King *et al.*, 2017), the use of AMPS in this study is justified. The results presented here are similar to findings by Cape *et al.* (2015) over the northern AP, and extend the understanding of the temporal and spatial distribution of föhn winds over the LCIS.

The clearest temporal signature was the peak in föhn frequency during spring (SON). In 2010, over 65% of föhn conditions were identified during spring, equating to 32 days of föhn conditions, or 34% of the season. This is consistent with findings by Cape *et al.* (2015), despite a different föhn-identification method being used, over Larsen B ice shelf and the northern AP, where föhn occurrence peaks in spring. Over the northern AP, the spring peak in föhn frequency was closely correlated to the position and strength of the Amundsen Sea low (ASL; Cape *et al.*, 2015). The large number of föhn conditions during spring coincides with a more southwesterly (away from the AP) location of the ASL and a deepening of the low pressure system, which deflects stronger and more frequent airflow over the AP (Hosking *et al.*, 2013). Cape *et al.* (2015) also identified that there was a strong positive correlation between the frequency of föhn conditions and the strengthening index of the Southern Annular Mode (SAM). The link between SAM and föhn winds was hypothesised by Marshall *et al.* (2006). The strengthening positive index of SAM since the 1960s is believed to have increased the frequency of föhn winds over the AP. Due to the relatively short observational period in the current study, links to large-scale variability have not been investigated.

The impact of föhn conditions on the ice shelf is potentially amplified during spring, compared to other seasons. During spring the air temperatures over the LCIS are around −14 °C, and melting is relatively infrequent during non-föhn periods. However, the high föhn frequency in spring increases the likelihood of air temperatures reaching above freezing, and therefore increases the potential for föhn-induced surface melting. An individual föhn event during November 2010, was responsible for prolonged surface melt observed at AWS2 (Kuipers Munneke *et al.*, 2012).

Although the föhn events were short (6 or 12 hr), they often grouped together in rapid succession (Figure 4). This can aggregate the impact on the surface, and cause prolonged melting. In a study by Barrett *et al.* (2008), multiple consecutive föhn events had an impact on the soil temperatures and surface melting in the McMurdo dry valleys, which outlived the duration of the föhn events themselves. Luckman *et al.* (2014) found that a northwest to southeast gradient in surface melt on the LCIS explained the ice shelf densification, and sustained melt pond observed in this region. Repetitive föhn events lower the albedo of the surface ice through melt ponds, leading to a positive feedback of additional melt. Luckman *et al.* (2014) hypothesized that the reduction in melt extent after the summer season was likely due to refreezing and snow accumulation or through percolation of the water into crevasses. The repeated melting of surface ice reduces the firn air space available for the meltwater, forcing the water to pond on the surface, or eventually drain into crevasses within the ice shelf (Kuipers Munneke *et al.*, 2014). This is considered

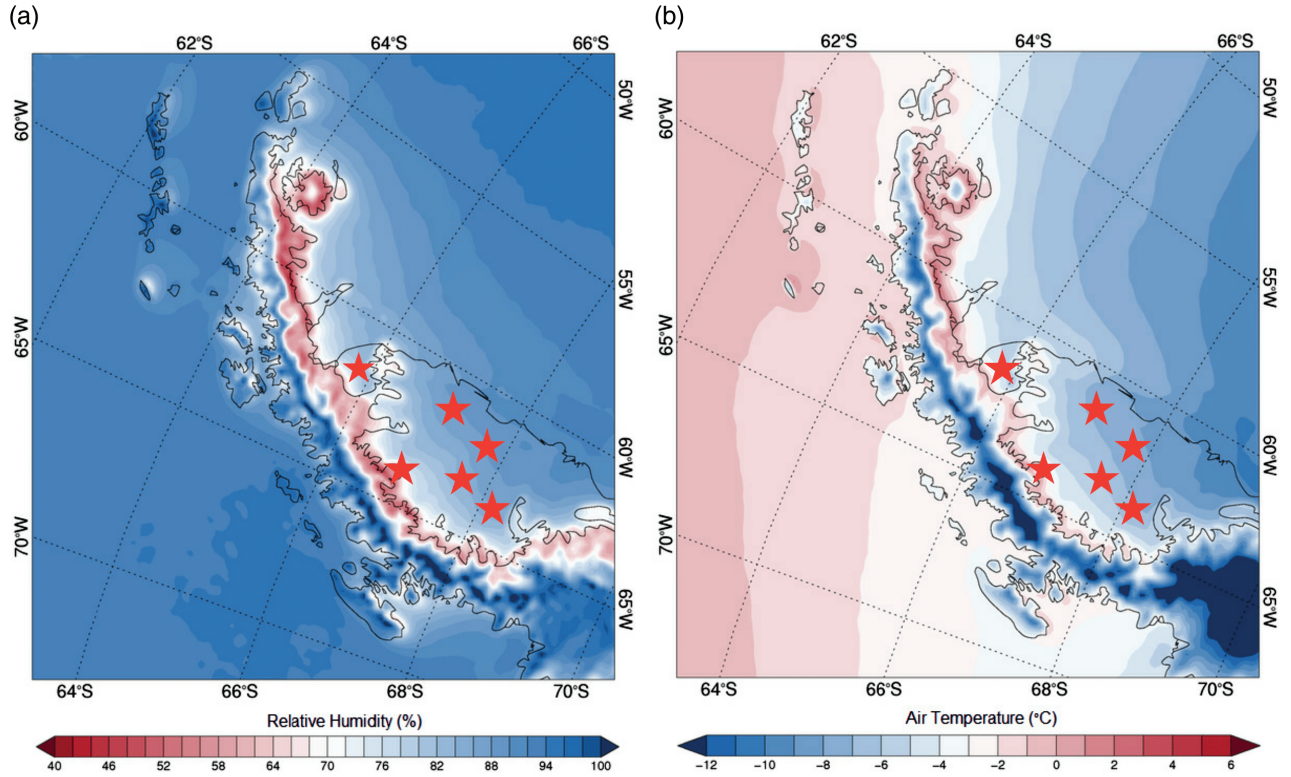

FIGURE 7 Composites of (a) the near-surface relative humidity and (b) air temperature modelled by AMPS during all föhn conditions from 2009 to 2012. Stars indicate AWS locations

a good indicator of ice shelf instability and a precursor for collapse (Kuipers Munneke *et al.*, 2014). The gradient in surface melting identified by Luckman *et al.* (2014) on the LCIS was attributed to more frequent and stronger föhn events, as subsequently identified in the current study.

Usually the föhn air propagates across the ice shelf in a northwest to southeast direction. Föhn conditions were observed at some point during the study period at all locations on the LCIS, including AWS6, the most southerly location. The impact of the föhn conditions on the near-surface characteristics varied by location. During times when föhn conditions were identified at Cole Peninsula, the air temperature over the ice shelf observed by the other AWSs increased by 3.5 K, highlighting the widespread impact of föhn events. Föhn-induced surface melting has been observed over 100 km from the AP during individual cases (Kuipers Munneke *et al.*, 2012). The identification of föhn conditions, and the potential for surface melting at AWS6, is the furthest south that föhn conditions have been observed over the AP. Combining this study with Cape *et al.* (2015) creates an ice-shelf-wide (64.8°S to 68.1°S) picture of föhn conditions and their frequency. The current study has focused on the spatial and temporal variability of the föhn conditions and has found that many features (including frequency, duration and strength) have localized signatures. Detailed assessment of the impact of a number of föhn conditions on the surface energy balance and surface melting is presented by King *et al.* (2017), and a multi-year assessment is in progress. Combining previous findings by Luckman *et al.* (2014), King *et al.* (2017) and Lenaerts *et al.* (2017) with the results of the current study, the impact of föhn conditions on the surface melting of the LCIS is thought to be considerable.

ACKNOWLEDGEMENTS

The authors would like to acknowledge the Natural Environment Research Council (NERC) grant NE/G014124/1 "Orographic Flows and the Climate of the Antarctic Peninsula", and NERC funded studentship NE/L501633/1. We thank NCAR for giving us access to the AMPS forecast archives, IMAU and CIRES for the AWS data and the British Antarctic Survey staff at Rothera Research Station for field support.

ORCID

Jenny V. Turton http://orcid.org/0000-0003-0581-8293

REFERENCES

Bannister, D. (2015) *Foehn winds on South Georgia and their impact on regional climate*. PhD thesis, Norwich, University of East Anglia.

Barrett, J.E., Virginia, R.A., Wall, D.H., Doran, P.T., Fountain, A.G., Welch, K.A. and Lyons, W.B. (2008) Persistent effects of a discrete warming event on a polar desert ecosystem. *Global Change Biology*, 14, 2249–2261. https://doi.org/doi:10.1111/j.1365-2486.2008.01641.x.

Bromwich, D.H., Hines, K.M. and Bai, L. (2009) Development and testing of Polar Weather Research and Forecasting model: 2. Arctic Ocean. *Journal of Geophysical Research*, 114, D08122. https://doi.org/doi:10.1029/2008JD010300.

Cape, M.R., Vernet, M., Skvarca, P., Marinsek, S., Scambos, T. and Domack, E. (2015) Foehn winds link climate-driven warming to ice shelf evolution in Antarctica. *Journal of Geophysical Research: Atmospheres*, 120, 11037–11057. https://doi.org/doi:10.1002/2015JD023465.

Cook, A.J. and Vaughan, D.G. (2010) Overview of areal changes of the ice shelves on the Antarctic Peninsula over the past 50 years. *The Cryosphere*, 4, 77–98. https://doi.org/doi:10.5194/tc-4-77-2010.

Dürr, B. (2003) *Automatisiertes Verfahren zur Bestimmung von Föhn in Alpentälern*. Zurich, Meteoschweiz. Technical Report 223.

Elvidge, A.D., Renfrew, I.A., King, J.C., Orr, A., Lachlan-Cope, T.A., Weeks, M. and Gray, S.L. (2015) Foehn jets over the Larsen C Ice Shelf, Antarctica. *Quarterly Journal of the Royal Meteorological Society*, 141, 698–713. https://doi.org/doi:10.1002/qj.2382.

Elvidge, A.D. and Renfrew, I.A. (2016) The causes of foehn warming in the lee of mountains. *Bulletin of the American Meteorological Society*, 97, 455–466. https://doi.org/doi:10.1175/BAMS-D-14-00194.1.

Elvidge, A.D., Renfrew, I.A., King, J.C., Orr, A. and Lachlan-Cope, T.A. (2016) Foehn warming distributions in nonlinear and linear flow regimes: a focus on the Antarctic Peninsula. *Quarterly Journal of the Royal Meteorological Society*, 142, 618–631. https://doi.org/doi:10.1002/qj.2489.

Gaffin, D.M. (2007) Foehn winds that produced large temperature differences near the Southern Appalachian mountains. *Weather and Forecasting*, 22, 145–159. https://doi.org/doi:10.1175/WAF970.1.

Grazioli, J., Madeleine, J.B., Gallée, H., Forbes, R.M., Genthon, C., Krinner, G. and Berne, A. (2017) Katabatic winds diminish precipitation contribution to the Antarctic ice mass balance. *Proceedings of the National Academy of Sciences of the United States of America*, 114, 10858–10863. https://doi.org/doi:10.1073/pnas.1707633114.

Hann, J. (1866) Zur Frage über den Ursprung des Föhn. *Zeitschrift der Österreich-ischen Gesellschaft für Meteorologie*, 1, 257–263.

Hines, K.M. and Bromwich, D.H. (2008) Development and testing of polar Weather Research and Forecasting (WRF) Model. Part I: Greenland ice sheet meteorology. *Monthly Weather Review*, 136, 1971–1989. https://doi.org/doi:10.1175/2007MWR2112.1.

Hogg, A.E. and Gudmundsson, G.H. (2017) Impacts of the Larsen C ice shelf calving event. *Nature Climate Change*, 7, 540–542. https://doi.org/doi:10.1038/nclimate3359.

Hosking, J.S., Orr, A., Marshall, G.J., Turner, J. and Phillips, T. (2013) The Influence of the Amundse-n-Bellingshausen Seas low on the climate of West Antarctica and its representation in coupled climate model simulations. *Journal of Climate*, 26, 6633–6648. https://doi.org/doi:10.1175/JCLI-D-12-00813.1.

Hubbard, B., Luckman, A., Ashmore, D.W., Bevan, S., Kulessa, B., Kuipers Munneke, P., Philippe, M., Jansen, D., Booth, A., Sevestre, H., Tison, J.-L., O'Leary, M. and Rutt, I. (2016) Massive subsurface ice formed by refreezing of ice-shelf melt ponds. *Nature Communications*, 7, 11897. https://doi.org/doi:10.1038/ncomms11897.

Jansen, D., Luckman, A.J., Cook, A., Bevan, S., Kulessa, B. and Hubbard, B. (2015) Brief communication: newly developing rift in Larsen C ice shelf presents significant risk to stability. *The Cryosphere*, 9, 1223–1227. https://doi.org/doi:10.5194/tc-9-1223-2015.

King, J.C., Kirchgaessner, A., Orr, A., Luckman, A., Bevan, S., Elvidge, A., Renfrew, I. and Kuipers Munneke, P. (2017) The impact of foehn winds on surface energy balance during the 2010–2011 melt season over Larsen C Ice Shelf, Antarctica. *Journal of Geophysical Research: Atmospheres*, 122, 12062–12076. https://doi.org/doi:10.1002/2017JD026809.

King, J.C., Gadian, A., Kirchgaessner, A., Kuipers Munneke, P., Lachlan-Cope, T.A., Orr, A., Reijmer, C., van den Broeke, M.R., van Wessem, J.M. and Weeks, M. (2015) Validation of the summertime surface energy budget of Larsen C Ice Shelf (Antarctica) as represented in three high-resolution atmospheric models. *Journal of Geophysical Research: Atmospheres*, 120, 1335–1347. https://doi.org/doi:10.1002/2014JD022604.

Kuipers Munneke, P., van den Broeke, M., King, J.C., Gray, T. and Reijmer, C. (2012) Near-surface climate and surface energy budget of Larsen C Ice Shelf, Antarctic Peninsula. *The Cryosphere*, 6, 353–363. https://doi.org/doi:10.5194/tc-6-353-2012.

Kuipers Munneke, P., Ligtenberg, S.R., Van Den Broeke, M.R. and Vaughan, D.G. (2014) Firn air depletion as a precursor of Antarctic ice-shelf collapse. *Journal of Glaciology*, 60, 205–214. https://doi.org/doi:10.3189/2014JoG13J183.

Lenaerts, J.T.M., Lhermitte, S., Drews, R., Ligtenberg, S.R.M., Berger, S., Helm, V., Smeets, C.J.P.P., van den Broeke, M.R., van de Berg, W.J., van Meijgaard, E., Eijkelboom, M., Eisen, O. and Pattyn, F. (2017) Meltwater produced by wind–albedo interaction stored in an East Antarctic ice shelf. *Nature Climate Change*, 7, 58–62. https://doi.org/doi:10.1038/nclimate3180.

Luckman, A., Elvidge, A., Jansen, D., Kulessa, B., Kuipers Munneke, P., King, J. and Barrand, N.E. (2014) Surface melt and ponding on Larsen C Ice Shelf and the impact of föhn winds. *Antarctic Science*, 26, 625–635. https://doi.org/doi:10.1017/S0954102014000339.

Marshall, G.J., Orr, A., van Lipzig, N.P.M. and King, J.C. (2006) The impact of a changing Southern Hemisphere annular mode on Antarctic Peninsula summer temperatures. *Journal of Climate*, 19, 5388–5404. https://doi.org/doi:10.1175/JCLI3844.1.

Miltenberger, A.K., Reynolds, S. and Sprenger, M. (2016) Revisiting the latent heating contribution to foehn warming – Lagrangian analysis of two foehn events over the Swiss Alps. *Quarterly Journal of the Royal Meteorological Society*, 142, 2194–2204. https://doi.org/doi:10.1002/qj.2816.

Morris, E. and Vaughan, D. (2003) Spatial and temporal variation of surface temperature on the Antarctic Peninsula and the limit of variability of ice shelves. In: Domack, E., Burnett, A., Leventer, A., Conley, P., Kirby, M. and Bindschadler, R. (Eds.) *Antarctic Peninsula Climate Variability: Historical and Paleoenvironmental Perspective*. Washington, DC: American Geophysical Union, pp. 61–68.

Richner, H., Baumann-Stanzer, K., Benech, B., Berger, H., Chimani, B., Dorninger, M., Drobinski, P., Furger, M., Gubser, S., Gutermann, T., Häberli, C., Häller, E., Lothon, M., Mitev, V., Ruffieux, D., Seiz, G., Steinacker, R., Tschannett, S., Vogt, S. and Werner, R. (2005) Unstationary aspects of foehn in a large valley. Part I: operational set-up, scientific objectives and analysis of the cases during the special observing period of the MAP subprogramme FORM. *Meteorology and Atmospheric Physics*, 92, 255–284. https://doi.org/doi:10.1007/s00703-005-0134-y.

Scambos, T.A. (2004) Glacier acceleration and thinning after ice shelf collapse in the Larsen B embayment, Antarctica. *Geophysical Research Letters*, 31(L18402). https://doi.org/doi:10.1029/2004GL020670.

Scambos, T.A., Hulbe, C., Fahnestock, M. and Bohlander, J. (2000) The link between climate warming and break-up of ice shelves in the Antarctic Peninsula. *Journal of Glaciology*, 46, 516–530. https://doi.org/doi:10.3189/172756500781833043.

Speirs, J.C., McGowan, H.A., Steinhoff, D.F. and Bromwich, D.H. (2013) Regional climate variability driven by foehn winds in the McMurdo dry valleys, Antarctica. *International Journal of Climatology*, 33, 945–958. https://doi.org/doi:10.1002/joc.3481.

Steinhoff, D.F., Bromwich, D.H., Speirs, J.C., McGowan, H.A. and Monaghan, A.J. (2014) Austral summer foehn winds over the McMurdo dry valleys of Antarctica from Polar WRF. *Quarterly Journal of the Royal Meteorological Society*, 140, 1825–1837. https://doi.org/doi:10.1002/qj.2278.

Turton, J., Kirchgaessner, A., King, J. and Ross, A. (2017) Does high-resolution modelling improve the spatial analysis of foehn flow over the Larsen C ice shelf? *Weather*, 72, 192–196.

Vaughan, D.G., Marshall, G.J., Connolley, W.M., Parkinson, C., Mulvaney, R., Hodgson, D.A., King, J.C., Pudsey, C.J. and Turner, J. (2003) Recent rapid regional climate warming on the Antarctic Peninsula. *Climatic Change*, 60, 243–274. https://doi.org/doi:10.1023/A:1026021217991.

Vergeiner, J. (2004) *South foehn studies and a new foehn classification scheme in the Wipp and Inn valley*. PhD thesis. University of Innsbruck, Austria.

Wilson, A.B., Bromwich, D.H. and Hines, K.M. (2012) Evaluation of Polar WRF forecasts on the Arctic System Reanalysis domain: 2. Atmos-pheric hydrologic cycle. *Journal of Geophysical Research*, 117, D04107. https://doi.org/10.1029/2011JD016765.

SUPPORTING INFORMATION

Additional supporting information may be found online in the Supporting Information section at the end of the article.

How to cite this article: Turton JV, Kirchgaessner A, Ross AN, King JC. The spatial distribution and temporal variability of föhn winds over the Larsen C ice shelf, Antarctica. *Q J R Meteorol Soc*. 2018;144:1169–1178. https://doi.org/10.1002/qj.3284